

Article

Corrosion Inhibition of Mild Steel in Hydrochloric Acid Environment Using Terephthaldehyde Based on Schiff Base: Gravimetric, Thermodynamic, and Computational Studies

Bahaa Sami Mahdi ¹, Muna Khethier Abbass ¹, Mustafa Khudhair Mohsin ², Waleed Khalid Al-azzawi ³, Mahdi M. Hanoon ¹, Mohammed Hliyil Hafiz Al-kaabi ⁴, Lina M. Shaker ⁵, Ahmed A. Al-amieriy ^{5,6,*}, Wan Nor Roslam Wan Isahak ^{5,*}, Abdul Amir H. Kadhum ⁷ and Mohd S. Takriff ⁸

¹ Production Engineering and Metallurgy, University of Technology-Iraq, Baghdad 10001, Iraq; 70078@uotechnology.edu.iq (B.S.M.); muna.k.abbass@uotechnology.edu.iq (M.K.A.); 70182@uotechnology.edu.iq (M.M.H.)

² The Supreme National Authority for Accountability and Justice, Baghdad 10001, Iraq; faydalaa1991@gmail.com

³ Department of Medical Instruments Engineering Techniques, Al-Farahidi University, Baghdad 10001, Iraq; waleed.khalid@alfarahidiuc.edu.iq

⁴ College of Industrial Management of Oil and Gas, Basrah University of Oil and Gas, Basrah 61001, Iraq; drmh1962@gmail.com

⁵ Department of Chemical and Process Engineering, Faculty of Engineering and Built Environment, Universiti Kebangsaan Malaysia (UKM), Bangi P.O. Box 43000, Malaysia; linamohammed91@gmail.com

⁶ Energy and Renewable Energies Technology Center, University of Technology-Iraq, Baghdad 10001, Iraq

⁷ Faculty of Medicine, University of Al-Ameed, Karbala 56001, Iraq; amir1719@gmail.com

⁸ Chemical and Water Desalination Engineering Program, Department of Mechanical & Nuclear Engineering, College of Engineering, University of Sharjah, Sharjah 26666, United Arab Emirates; sobritakriff@ukm.edu.my

* Correspondence: dr.ahmed1975@ukm.edu.my (A.A.A.-a.); wannorroslam@ukm.edu.my (W.N.R.W.I.)



Citation: Mahdi, B.S.; Abbass, M.K.; Mohsin, M.K.; Al-azzawi, W.K.; Hanoon, M.M.; Al-kaabi, M.H.H.; Shaker, L.M.; Al-amieriy, A.A.; Isahak, W.N.R.W.; Kadhum, A.A.H.; et al. Corrosion Inhibition of Mild Steel in Hydrochloric Acid Environment Using Terephthaldehyde Based on Schiff Base: Gravimetric, Thermodynamic, and Computational Studies.

Molecules **2022**, *27*, 4857.

<https://doi.org/10.3390/molecules27154857>

Academic Editors: Lukman Olawale Olasunkanmi and Eno E. Ebenso

Received: 13 June 2022

Accepted: 27 July 2022

Published: 29 July 2022

Publisher's Note: MDPI stays neutral with regard to jurisdictional claims in published maps and institutional affiliations.



Copyright: © 2022 by the authors. Licensee MDPI, Basel, Switzerland. This article is an open access article distributed under the terms and conditions of the Creative Commons Attribution (CC BY) license (<https://creativecommons.org/licenses/by/4.0/>).

Abstract: Using traditional weight-loss tests, as well as different electrochemical techniques (potentiodynamic polarization and electrochemical impedance spectroscopy), we investigated the corrosion-inhibition performance of 2,2'-(1,4-phenylenebis(methanylylidene)) bis(N-(3-methoxyphenyl) hydrazinecarbothioamide) (PMBMH) as an inhibitor for mild steel in a 1 M hydrochloric acid solution. The maximum protection efficacy of 0.0005 M of PMBMH was 95%. Due to the creation of a protective adsorption layer instead of the adsorbed H₂O molecules and acidic chloride ions, the existence of the investigated inhibitor reduced the corrosion rate and increased the inhibitory efficacy. The inhibition efficiency increased as the inhibitor concentration increased, but it decreased as the temperature increased. The PMBMH adsorption mode followed the Langmuir adsorption isotherm, with high adsorption-inhibition activity. Furthermore, the value of the ΔG_{ads}^o indicated that PMBMH contributed to the physical and chemical adsorption onto the mild-steel surface. Moreover, density functional theory (DFT) helped in the calculation of the quantum chemical parameters for finding the correlation between the inhibition activity and the molecular structure. The experimental and theoretical findings in this investigation are in good agreement.

Keywords: terephthaldehyde; Schiff base; corrosion inhibitor; weight loss; DFT; EIS

1. Introduction

In view of its excellent mechanical durability, easy processing, and low production cost, iron and its alloys are applied as materials for construction in a variety of industrial uses, including petroleum, power plants, and chemical industries [1,2]. Steel comes into contact with corrosive environments in a variety of ways, including acidic solutions during etching, acid pickling, acid descaling, acid cleaning, and oil-well acidification [3]. Steel alloys react readily in acidic conditions, converting from a metallic to an ionic state, which

results in significant economic loss. As a result, there is a pressing need to develop effective corrosion-control technologies.

The use of corrosion inhibitors is one of the approaches [4–6]. Corrosion inhibitors are categorized based on their chemical structures, modes of action, and other factors. Organic corrosion inhibitors are among the most frequently used groups, and they have gained prominence due to their simplicity of synthesis at a low cost and their good protective capabilities. The preventative strategy is attributed to adsorption onto the mild-steel substrate, which obstructs corroding sites. The production of a protective barrier between the corrosive solution and the mild-steel surface prevents the mild steel from dissolving in the corrosive environment [7,8]. Corrosion is a significant issue in manufacturing, water, and circulation systems. Inhibitors are added to corrosive environments to prevent corrosion.

Organic inhibitors include heteroatoms, such as N, O, S, and P, and they have been shown to be effective corrosion inhibitors in a variety of acidic solutions, both practically and theoretically [9,10]. The efficiency of these inhibitors can be related to their strong polarizability and decreased electronegativity, which allow them to cover vast metal surfaces and efficiently transfer electrons to the vacant orbitals of atoms [11]. Furthermore, organic inhibitors that contain nitrogen are effective corrosion-protection materials for alloys in HCl solutions, whereas sulfur-containing compounds are effective inhibitors in H₂SO₄ solutions. For both media, nitrogen- and sulfur-containing compounds act as ideal corrosion inhibitors [12]. The type of the distinctive inhibitor layer formed on the mild-steel substrate, as well as the quantity and nature of the adsorption centers attributed to the adsorption mechanism, determine the action of any inhibitor for any specific metallic alloy in severely corrosive solutions.

Generally, the inhibitory efficiency of inhibitors with various heteroatoms follows the inverse sequence of the respective electronegativity values. Therefore, the inhibitory effectiveness of S, N, O, and P follows the order: oxygen (O) < nitrogen (N) < sulfur (S) < phosphorus (P) [13]. When organic molecules are present in acidic conditions, the electrochemical behavior of the acidic medium is frequently altered. In other words, it reduces the solution's aggressiveness. Phosphorus, sulfur, oxygen, and nitrogen heteroatoms are found in the most commonly utilized heterocyclic compounds, and they effectively participate in the adsorption centers. We concentrated on the synthesis of a Schiff base generated from terephthalaldehyde, namely, 2,2'-(1,4-phenylenebis(methanylylidene))bis(N-(3-methoxyphenyl)hydrazinecarbothioamide) (PMBMH), (Figure 1), as an acid corrosion inhibitor for mild steel, which works as a multifunctional protective agent. Terephthalaldehyde and 4-(meta-methoxyphenyl)-3-thiosemicarbazide react to produce the chemical composition of the produced compounds. Because of these properties, the tested inhibitor has the potential to be a novel corrosion inhibitor. In continuation of the research on the advancement of Schiff bases as efficient anticorrosion compounds in HCl solution, the present investigation discusses the inhibition efficiency of PMBMH on mild-steel corrosion in a corrosive medium by using a weight-loss technique, potentiodynamic polarization, electrochemical impedance spectroscopy, and scanning electron microscopy. The experimental results are correlated with the quantum chemical calculations employing density functional theory (DFT) to explain how the inhibitor works to effectively coordinate with the mild-steel surface.

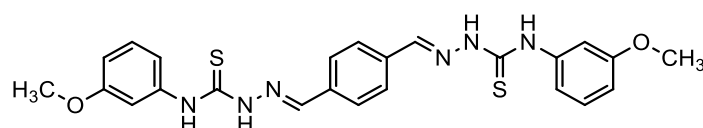


Figure 1. The chemical structure of PMBMH.

2. Results and Discussion

2.1. Gravimetric Techniques

The rates of the corrosion and inhibition efficiency of the tested corrosion inhibitor at different concentrations (0.0001, 0.0002, 0.0003, 0.0004, 0.0005, and 0.0010 M) and various

temperatures (303–333 K) were analyzed by weight-loss measurements, and the experimental findings are presented in Figures 2 and 3. PMBMH, the synthesized inhibitor, has been proven to be quite effective at inhibiting mild-steel corrosion. Figure 2 shows the effect of changing the PMBMH concentration on the corrosion rate, and thus the inhibition efficiency. At 303 K, the weight-loss measurements were taken. The corrosion rate decreased as the inhibitor concentration increased, and the inhibition improved, as indicated in Figure 2. This shows that, when the concentration rises, inhibitor molecules are essentially adsorbed to a higher extent onto the metal substrate, which results in broader surface coverage. As a result, it is clear that the performance of the inhibition was concentration dependent. Hence, the metal's contact with the acid solution was limited. The PMBMH showed the highest inhibition efficacy at 0.0005, and the inhibition effectiveness was found to be 95.7%.

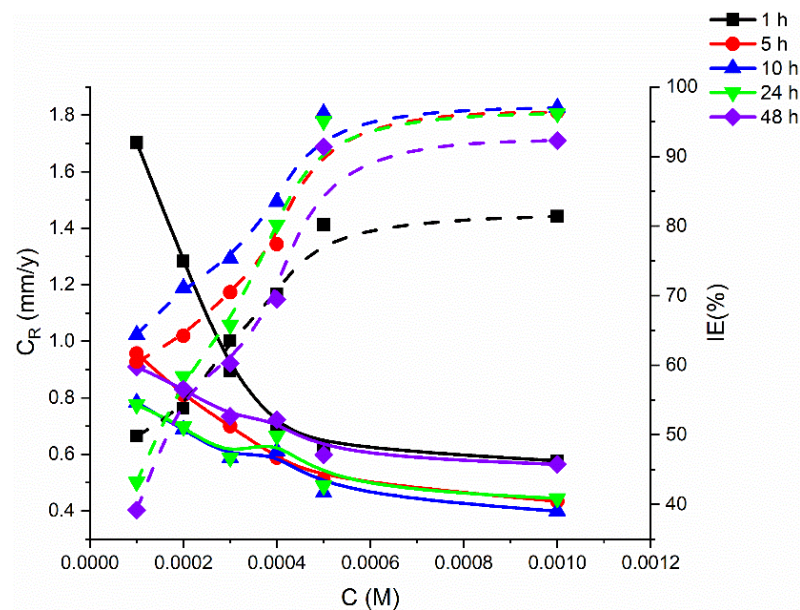


Figure 2. Gravimetric-curve relationship of metal coupons in 1 M HCl between corrosion rate and inhibition efficiency: different exposure periods at 303 K.

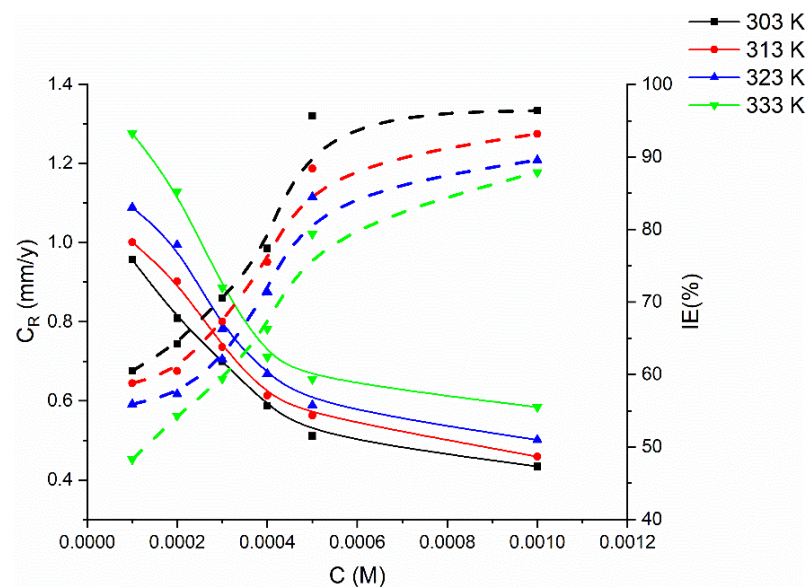


Figure 3. Gravimetric-curve relationship of metal coupons in 1 M HCl between corrosion rate and inhibition efficiency against concentration of PMBMH at different temperatures for 5 h exposure period.

Adsorbed inhibitor molecules control and/or block reaction sites, protecting the mild-steel surface from the corrosive medium. The inhibitor possesses many ion pairs of electrons, such as those on sulfur and nitrogen atoms, and the pi-electrons, which are coordinately bound with iron atoms on the coupon surface, which may be able to prevent corrosion. In other words, the excellent inhibition efficiency of PMBMH may be due to the addition of electron-donating functional groups, such as the amine, thione, imine, and aromatic rings, which improve the ability of inhibitor molecules to transfer electrons to the unoccupied d-orbitals of iron, thereby slowing the corrosion process. It is very well recognized that the effectiveness of inhibitor molecules increases with its electron-donating-power capacity. Increasing the inhibitor concentration does not result in a noticeable change in the percentage inhibition, as shown in Figure 2. This could be owing to the surface's saturation. As a result, the optimum concentration is determined as 0.0005 M.

The present inhibitor's PMBMH inhibitory performance in HCl can be compared to those of earlier inhibitor studies that use heterocyclic organic molecules as corrosion inhibitors to protect metals from corrosive solutions. As shown in Table 1, most of the tested heterocyclic organic compounds have significant inhibitory efficacy. PMBMH has the strongest inhibitory ability of the heterocyclic organic compounds reported in Table 1 [14–31], with a performance equivalent to those reported in [15,23,26,28]. As the concentration of PMBMH increases, the rate of corrosion decreases, and the inhibitive efficacy improves. This could be because the inhibitor's adsorption coverage on metal substrates increases as the PMBMH concentration rises.

2.2. Effect of Time

With a concentration of 0.0005 M, a temperature of 303 K, and a 5 h immersion time, the inhibitor had a maximum protection efficacy of 95.7%. The weight loss and corrosion rate increased with the immersion duration for the tested specimens, as well as at all the examined dosages of the examined inhibitor [31], according to the experimental observations shown in Figure 2. The corrosion rate increased marginally after 24 h of exposure in the presence of the studied inhibitor. As a result, the extended immersion duration in the acidic medium might be related to the minor increase in corrosion. For different inhibitor concentrations, Figure 2 displays a graph of the rate of corrosion and the protection performance against the immersion time (hours). The inhibition efficiency increased sharply with the lengthening of time for all inhibitor concentrations, as shown in these results. Then, based on the concentration of the inhibitor, a decrease in the value was detected after 24 h. The rate of corrosion increased marginally after 24 h of immersion with the addition of the examined inhibitor. As a consequence, the extended exposure duration in the HCl medium may be related to the slight increase in corrosion.

For different inhibitor concentrations, Figure 2 depicts a graph of the corrosion rate versus the protection efficacy (percentage) over time (hours). The protection efficacy increased sharply with increasing time for all the inhibitor concentration levels, as shown in these results. Then, based on the concentration of the inhibitor, a decrease in the value was detected after 24 h. The improvement in the protective efficacy is attributed to the increased surface coverage due to the adsorption of the inhibitor molecules onto the surface of the mild steel. By inhibiting the active sites, the adsorption barrier protects the mild-metal surfaces from the acid medium.

2.3. Effect of Temperature

Temperature has a significant impact on the corrosion rate and inhibiting efficacy, and particularly in an acidic medium. The rate of corrosion increases dramatically with rising temperature. The corrosion rate and inhibitory efficacy of the examined inhibitor were evaluated at varying temperature ranges (from 303 to 333 K) to fully understand its protection performance (Figure 3). At 303 K, the examined inhibitor had the maximum inhibitory efficacy, which gradually decreased as the temperature was raised. At the highest temperature, the tested inhibitor performed poorly in terms of protection. This

finding indicates that the increase in temperature did not enable physical interactions (physisorption), which resulted in a reduction in the protective efficacy.

Table 1. PMBMH inhibition was statistically compared to the efficacy of other heterocyclic organic inhibitors that had previously been investigated.

Corrosion Inhibitor	Metal	Acid	IE%	Ref.
PMBMH	Mild steel	HCl	95.7	-
(E)-N0-(2,4-dimethoxybenzylidene)-2-(6-methoxynaphthalen-2-yl)propanehydrazide	Mild steel	HCl	95	[14]
N0-cyclohexylidene-2-(6-methoxynaphthalen-2-yl)propanehydrazide	Mild steel	HCl	86	[14]
Furoin thiosemicarbazone	Mild steel	HCl	98.7	[15]
2-pyridinecarboxaldehyde thiosemicarbazone	Mild steel	HCl	89.7	[16]
4-pyridinecarboxaldehyde thiosemicarbazone	Mild steel	HCl	85.5	[16]
clozapine	Mild steel	HCl	96	[17]
5-hexylsulfanyl-1,2,4-triazole	Mild steel	HCl	97	[18]
triglycidyl ether of triethoxy triazine	Carbon steel	HCl	88	[19]
N-propargyl saccharin	C38 steel	HCl	90	[20]
N-(2-aminophenyl)-2-(5-methyl-1H-pyrazol-3-yl)acetamide	C38 steel	HCl	93	[21]
dodecyl vanillin-glycine Schiff base	Carbon steel	H ₂ SO ₄	74.4	[22]
hexadecyl vanillin-glycine Schiff base	Carbon steel	HCl	78.5	[22]
octadecyl vanillin-glycine Schiff base	Carbon steel	HCl	80.8	[22]
oleic acid vanillin-glycine Schiff base	Carbon steel	HCl	81.9	[22]
3-(3-formyl-4-hydroxy-1-phenylazo)-1,2,4-triazole	Copper	HNO ₃	97	[23]
3-(2-hydroxy-5-methyl-1-phenylazo)-1,2,4-triazole	Copper	HNO ₃	95.8	[23]
3-(4-hydroxy-1-phenylazo)-1,2,4-triazole	Copper	HNO ₃	97.2	[23]
2-amino-7-hydroxy-4-phenyl-1,4-dihydroquinoline-3-carbonitrile	Mild steel	HCl	93.3	[24]
2-amino-7-hydroxy-4-(p-tolyl)-1,4-dihydroquinoline-3-carbonitrile	Mild steel	HCl	92.8	[24]
2-,2-amino-7-hydroxy-4-(4-methoxyphenyl)-1,4-dihydroquinoline-3-carbonitrile	Mild steel	HCl	96.6	[24]
2-amino-4-(4-(dimethylamino)phenyl)-7-hydroxy-1,4-dihydroquinoline-3-carbonitrile	Mild steel	HCl	98	[24]
5-Styryl-2,7-dithioxo-2,3,5,6,7,8-hexahydropyrimido[4,5-d]pyrimidin-4(1H)one	Carbon steel	HCl	89.1	[25]
5-(2-Hydroxyphenyl)-2,7-dithioxo-2,3,5,6,7,8-hexahydropyrimido[4,5-d]pyrimidin-4(1H)one	N80 steel	HCl	73.1	[25]
5-(2,5-dimethylthiophen-3-yl)-4-(4-(6-(2,5-dimethylthiophen-3-yl)-2-hydroxypyrimidin-4-yl)phenyl)pyrimidin-2-ol	Mild steel	H ₂ SO ₄	98.3	[26]
5-(2,5-dimethylthiophen-3-yl)-4-(4-(6-(2,5-dimethylthiophen-3-yl)-2-mercaptopyrimidin-4-yl)phenyl)pyrimidin-2-thiol	Mild steel	H ₂ SO ₄	99.3	[26]
2-chloropyrimidine	Cold rolled steel	HNO ₃	14.5	[27]
2-hydroxypyrimidine	Cold rolled steel	HNO ₃	23.0	[27]
2-bromopyrimidine	Cold rolled steel	HNO ₃	27.2	[27]
2-aminopyrimidine	Cold rolled steel	HNO ₃	35.0	[27]
2-mercaptopyrimidine	Cold rolled steel	HNO ₃	99.1	[27]
2-((6-methyl-2-ketoquinone-3-yl)methylene)hydrazinecarbothioamide	Mild steel	HCl	95.8	[28]
4-(6-methylcoumarin)acetohydrazide	Mild steel	HCl	94.5	[29]
4-(Benzoimidazole-2-yl)pyridine	Mild steel	HCl	93.8	[30]
5,5'-(1,4-phenylene)bis(N-phenyl-1,3,4-thiadiazol-2-amine)	Mild steel	HCl	94	[31]

Arrhenius Equation (1) was used to calculate the activation parameters of the corrosion process (Figure 4):

$$\log C_R = \log K - (E_a/2.303RT) \quad (1)$$

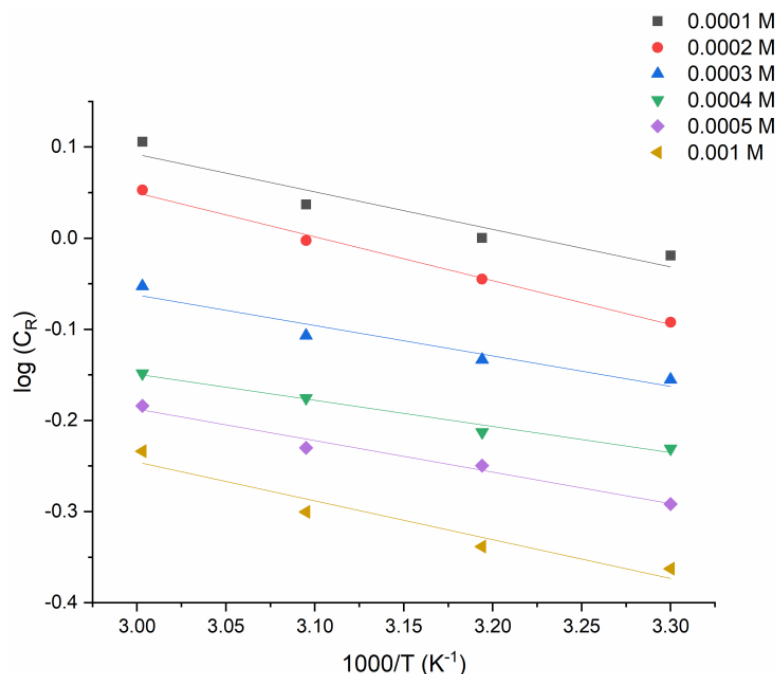


Figure 4. The $\log(C_R)$ versus $1/T$ graph for the various concentrations of PMBMH and different temperatures.

The fact that inhibitory processes have a higher activation energy than uninhibited ones implies that the dissolution of mild steel takes time. Furthermore, when the inhibitor concentration increased, so did the activation energy. This means that the inhibitor acts as a physical barrier to the corrosion process, which becomes stronger as the concentration becomes higher. The adsorption of inhibitor molecules onto the metal surface reduces as the temperature rises, and, as a consequence, the corrosion rates rise. According to the modified Arrhenius equation (Equation (2)), from the graph of $\log C_R/T$ versus $1/T$ for the tested metal that dissolves in the corrosion solution, it is possible to find the values of the enthalpy of activation (ΔH_a) and entropy of activation (ΔS_a):

$$\log \left\{ \frac{C_R}{T} \right\} = \left\{ \log \left[\frac{R}{Nh} \right] + \left[\frac{\Delta S_a}{2.303R} \right] \right\} - \left[\frac{\Delta H_a}{2.303RT} \right] \quad (2)$$

where N is the Avogadro's number, and h is the Planck's constant.

A plot of $\log C_R/T$ versus $1/T$ is shown in Figure 5. The activation-enthalpy (ΔH_a) and activation-entropy (ΔS_a) values obtained from the slope of Figure 5, and the intercept, are shown in Table 2.

The endothermic nature of dissolving mild steel is demonstrated by the positive ΔH_a values. The low rate of corrosion is primarily due to the kinetic properties of activation, as indicated by the rise in the ΔH_a with the rising inhibitor concentration. The values of the activation enthalpy without and with the addition (0.0005 M) of the examined inhibitor were ($60.43 \text{ kJ}\cdot\text{mol}^{-1}$) and ($43.76 \text{ kJ}\cdot\text{mol}^{-1}$), respectively (Table 2), as estimated from the slope of Figure 5. The values of the activation entropy without and with the addition of the examined inhibitor were ($57.58 \text{ J}\cdot\text{mol}^{-1} \text{ K}^{-1}$) and ($140.46 \text{ J}\cdot\text{mol}^{-1} \text{ K}^{-1}$), respectively, as estimated based on the intercept of Figure 5. The mild-steel-dissolving process is endothermic, according to the positive ΔH_a values without and with the presence of the tested inhibitor.

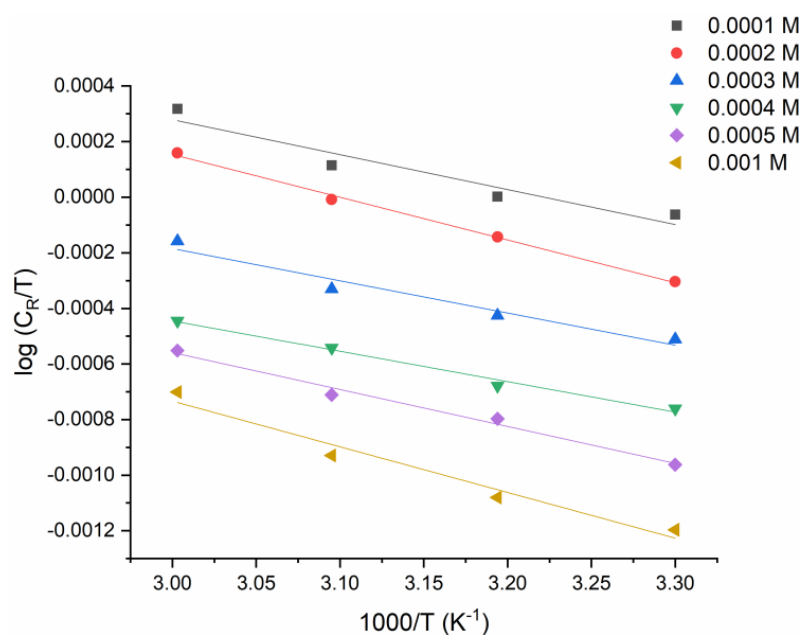


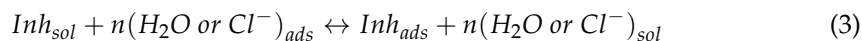
Figure 5. A plot of Arrhenius modified equations of $\log\left\{\frac{C_R}{T}\right\}$ versus $\frac{1}{T}$ for tested metal with different concentrations of the examined inhibitor.

Table 2. Isothermal parameter values for mild-steel coupon in 1 M HCl in the absence and presence of different concentrations of PMBMH.

C (M)	E_a (kJ·mol ⁻¹)	ΔH_a (kJ·mol ⁻¹)	ΔS_a (J·mol ⁻¹ K ⁻¹)
Blank	63.11	60.43	57.58
0.0001	51.46	52.65	123.54
0.0002	47.85	50.45	120.43
0.0003	45.35	47.67	124.43
0.0004	43.63	45.73	131.84
0.0005	41.78	43.76	140.46
0.001	39.85	42.10	151.65

2.4. Adsorption Isotherm

The quasi-substitution mechanism, according to Equation (3), which occurs at the electrode/electrolyte interface between the inhibitor molecules and the water or chloride ion, controls the competitive adsorption process:



where Inh_{sol} is the inhibitor molecules in the aqueous solution, and Inh_{ads} is the adsorbed inhibitor molecules on the mild-steel surface.

The adsorption process is linked to the barrier-shielding layer covering the electrode surface (θ). Temkin, Frumkin, Flory–Huggins, and Langmuir adsorption isotherm models are used to fit the gravimetric measurements using the relationship (Equation (4)) between the inhibitor concentration (C_{inh}) and the surface coverage (θ). The more suited adsorption model was developed (the Langmuir adsorption isotherm (as seen in Figure 6)) considering the high correlation coefficient (R^2), which depicts the inhibitor-adsorption mechanism excellently, as per [32,33]:

$$\frac{C}{\theta} = \frac{1}{K_{ads}} + C \quad (4)$$

where θ represents the surface coverage, K_{ads} refers to the constant of the adsorption process, and C is the concentration of the tested inhibitor.

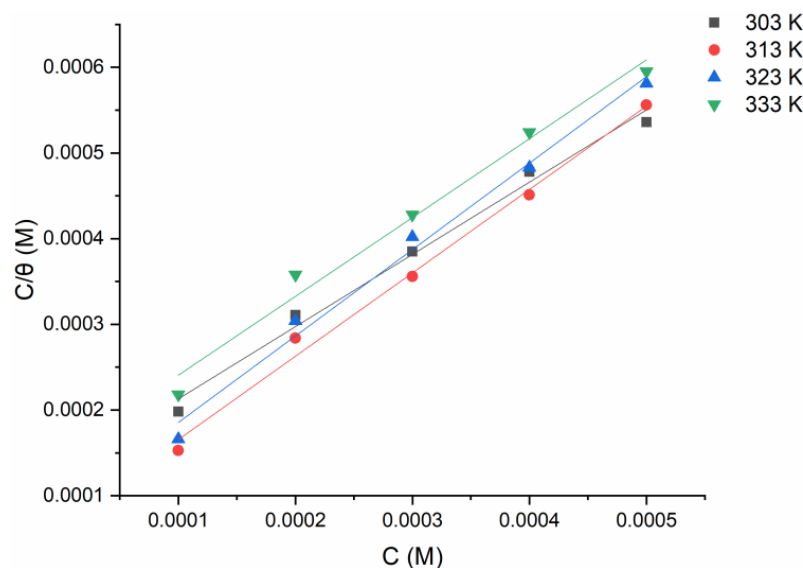


Figure 6. Langmuir adsorption model of tested inhibitor on the surface of mild steel in 1 M HCl at 303 K from the gravimetric data.

The free adsorption energy (ΔG_{ads}) was computed based on Equation (5):

$$\Delta G_{ads} = \left(\frac{1}{55.5} \right) \exp\left(\frac{K_{ads}}{RT} \right) \quad (5)$$

where the value 55.5 represents the molar concentration of water, T is the absolute temperature, and R is the universal gas constant.

The greater the value of the K_{ads} , the stronger the inhibitor's adsorption strength, and the lower the value of the ΔG_{ads} , the more spontaneous the adsorption process. The larger ΔG_{ads} value shows that the tested inhibitor has a chemical adsorption activity in which electrons are transferred from high-electron centers to the unoccupied 3d orbital of iron, which creates coordination bonds. The negative value of the adsorption free-energy charge decreases as the molecular weight of the tested inhibitor increases ($-38.21 \text{ kJ}\cdot\text{mol}^{-1}$), which corresponds to the gravimetric observations [34,35].

2.5. Potentiodynamic Polarization Measurements

Figure 7 displays the polarization curves for the tested coupon in 1.0 M corrosive media with different PMBMH concentrations at 303 K. Table 3 lists the data for the inhibitory performances, corrosion potential (E_{corr}), and corrosion current density (i_{corr}), in addition to the anodic (β_a) and cathodic (β_c) Tafel slopes. These numbers were generated using the Tafel fit technique offered by the Gamry Echem analyzer program, which uses a nonlinear chi-squared minimization to fit the data to the Stern–Geary equation. Equation (6) represents how the inhibition efficiency was estimated:

$$IE(\%) = \frac{i_{corr} - i_{corr(inh)}}{i_{corr}} \times 100 \quad (6)$$

where i_{corr} is the corrosion current density in the absence of PMBMH, and $i_{corr(inh)}$ is the corrosion current density in the presence of PMBMH.

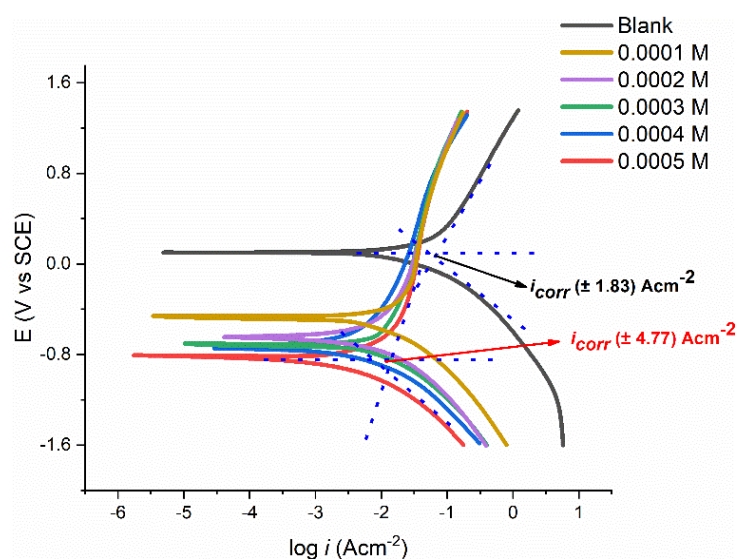


Figure 7. Polarization curves of tested coupons in 1 M HCl solution with different concentrations of PMBMH.

Table 3. Tafel parameters for tested coupon without and with the addition of various concentrations of PMBMH in 1 M HCl solution.

Conc. M	E_{corr} (V)	β_a (mV/dec)	β_c (mV/dec)	i_{corr} ($\mu\text{A}\cdot\text{cm}^{-2}$)	IE (%)
0.000	-0.46	120	140	663.8 ± 1.83	0
0.0001	-0.49	118.7	131.5	400.3 ± 5.03	67.1
0.0002	-0.52	131.5	133.2	230.1 ± 3.70	73.5
0.0003	-0.54	88.5	131.6	110.4 ± 2.93	84.7
0.0004	-0.51	67.5	100.5	90.4 ± 1.84	87.4
0.0005	-0.41	55.3	105.5	61.9 ± 4.77	92.3

When a compound's E_{corr} displacement exceeds 85 mV with respect to the E_{corr}^0 , it can be categorized as either a cathodic-type or anodic-type inhibitor [36,37]. The substances can be regarded as a mixed-type inhibitor because PMBMH causes the biggest displacement of the E_{corr} . Mild steel's anodic dissolution is slowed down and cathodic hydrogen evolution is postponed when PMBMH is added to the corrosive environment. Table 3 demonstrates that the values of the i_{corr} dropped when PMBMH was present. This finding suggests that the inhibition efficacy increases with the increasing PMBMH concentration, and the rate of corrosion reduces with the addition of the corrosion. The Tafel constant (β_a , β_c) values in the presence of PMBMH were barely varied, which proves that the PMBMH was in control of both processes. This finding also suggests that the hydrogen evolution or disintegration of mild steel was not impacted by the adsorbed molecules [38].

2.6. Electrochemical Measurements

Table 4 lists the experimental findings from the EIS analyses of mild-steel corrosion at 303 K, both without and with the addition of an inhibitor. Figure 8 displays Nyquist plots of the mild-steel-resistance spectrum in 1.0 M HCl in the absence and presence a varying PMBMH concentrations at 303 K. The inclusion of PMBMH caused the overall resistance to noticeably increase. Therefore, as seen in Figure 8, the presence of PMBMH in the HCl environment considerably altered the resistance responses of the mild steel. This variation was caused by an increase in the substrate resistance, which was related to an increase in the inhibitor's concentration. The Nyquist plots showed two loops in the impedance curves of mild steel in the presence and absence of PMBMH: one loop in the high-frequency range (HF), and one loop at an intermediate frequency (MF). Furthermore, at a lower frequency (LF), negligible inductive action was seen. The EIS instrument's limitations at

high frequencies with low resistances and charge-transfer operations were cited as the causes of the HF and MF loops, respectively. The relaxing mechanism of the adsorption of corrosion products or the adsorption of inhibitor molecules onto the mild-steel surface in acidic solution with and without the inhibitor, respectively, was said to be the cause of the inductive behavior seen in the LF region [39]. The following equation (Equation (7)) was used to obtain the inhibition efficiency (IE%) from the charge-transfer impedance:

$$IE(\%) = \frac{R'_{ct} - R_{ct}}{R'_{ct}} \times 100 \quad (7)$$

where R'_{ct} is the charge-transfer-resistance value in the presence of PMBMH, and R_{ct} is the charge-transfer-resistance value in the absence of PMBMH.

Table 4. EIS parameters for mild-steel coupon without and with the addition of various concentrations of PMBMH in 1 M corrosive solution.

Conc. (M)	R_s ($\Omega \text{ cm}^2$)	R_{ct} ($\Omega \text{ cm}^2$)	C_{dl} (μF)	IE%
Blank	2.047	54.85	493	0
0.0001	1.915	115.04	289	57.5
0.0002	1.836	158.68	311	69.6
0.0003	2.246	274.28	458	78.6
0.0004	1.703	323.8	641	87.6
0.0005	1.453	475.92	678	91.1

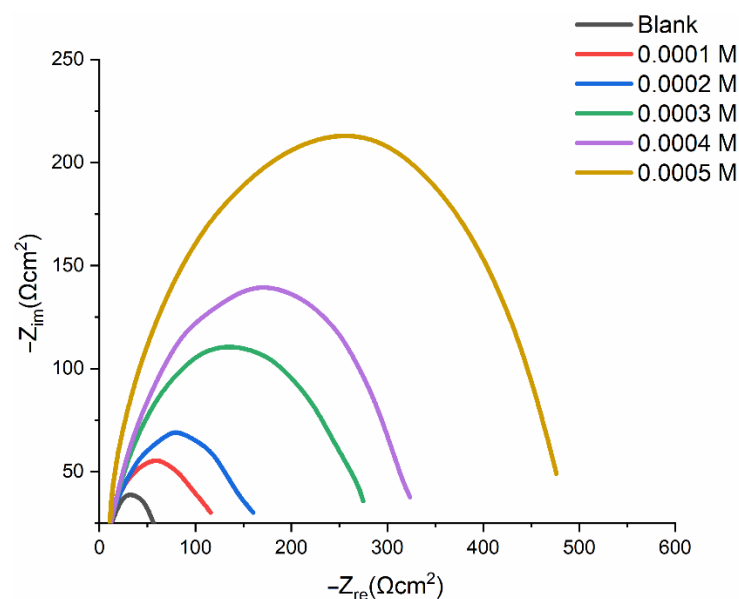


Figure 8. Nyquist plots of mild steel in 1 M HCl without and with the addition of various concentrations of PMBMH.

In the presence of PMBMH, it was discovered that the C_{dl} value rises from $323 \mu\text{F cm}^{-2}$ (0.0004 M) to $475 \mu\text{F cm}^{-2}$ (0.0005 M), which suggests that the layer thickness at 0.0005 M is greater than that at 0.0004 M.

According to Table 4, the charge-transfer resistance (R_{ct}) improved along with the inhibitor concentration. Systems that corrode gradually are attributed to large charge-transfer impedances [40]. Additionally, reduced metal capacitance is linked to enhanced inhibitor resistance. The observed rise in the C_{dl} , which was attributed to an increase in the local dielectric constant and/or the electrical double layer's thickness, indicates that the PMBMH adsorbed onto the interface between the material and the environment [41]. Inhibitor adsorption onto the most active adsorption sites may be to blame for the observed increase in the C_{dl} value in a corrosive solution in the presence of increasing concentrations

of PMBMH [42]. The homogeneity of the adsorbed PMBMH layer reduced due to the corrosion reaction.

Additionally, the findings demonstrated that, when the inhibitor concentration increased, so did the IE percent. This outcome exhibits the same pattern as the IE percent discovered through the weight-loss and potentiodynamic measurements. The equivalent circuit diagram for fitting the actual EIS results for hydrochloric acid in the presence and absence of the inhibitor is shown in Figure 9A,B. The solution resistance (R_s), a constant-phase element (CPE_{dl}), and the charge-transfer resistance are the circuit components for the data (Rct). The Rct value provided an indication of how well the electrons were moving over the contact. Rad was utilized as a model for the inhibitor adsorption in conjunction with a (CPE_{ad}) [43]:

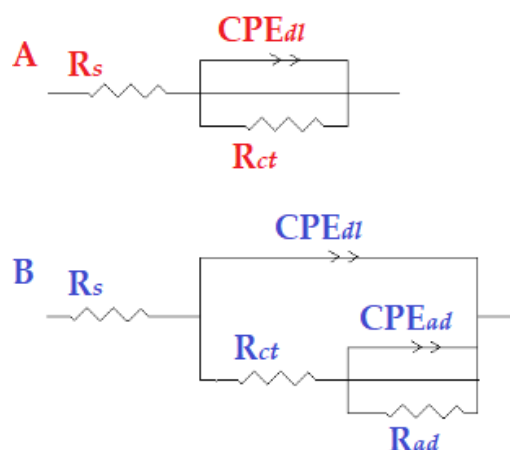


Figure 9. The model of equivalent circuit that was used to fit the experimental data (A) without and (B) with the addition of the tested inhibitor.

In Figure 9, R_s is the environment impedance; Rct is the charge-transfer impedance; CPE_{dl} signifies the double-layer constant-phase element; R_{ad} refers to the adsorbed-layer impedance; CPE_{ad} is the adsorbed-layer constant-phase element. Because an equivalent circuit is used to determine the simulated values and for comparison with experimental data, a CNLS (complex nonlinear least squares) simulation was used, as previously reported [44–46].

2.7. Surface Study

The scanning-electron-microscope (SEM) pictures of the mild-steel-coupon surface after immersion in the 1 M HCl medium, having (A) no inhibitor and (B) 0.0005 M PMBMH, for 5 h at 303 K, are demonstrated in Figure 10. The mild-steel-coupon surface corroded severely in the corrosive solution, as shown by the rough surface of the coupon surface in Figure 10A. The abundance of corrosion porous products can be obviously viewed on the mild-steel-coupon surface in Figure 10A. On the one hand, the mild-steel-coupon surface was damaged when immersed in the HCl environment, as demonstrated by Figure 10A. On the other hand, Figure 10B's depiction of the presence of an inhibitor shows that the mild-steel surface remained noticeably undamaged, inhibiting the corrosion process. This discovery confirmed the outcomes of the other experiments. As observed in Figure 10B, the mild-steel coupon immersed in 1 M HCl solution (in the presence of 0.0005 M of the tested inhibitor) had a smoother texture than the coupon exposed to the uninhibited acid solution, which indicates that the presence of the inhibitor protected the coupon surface from the corrosive environment's attack.

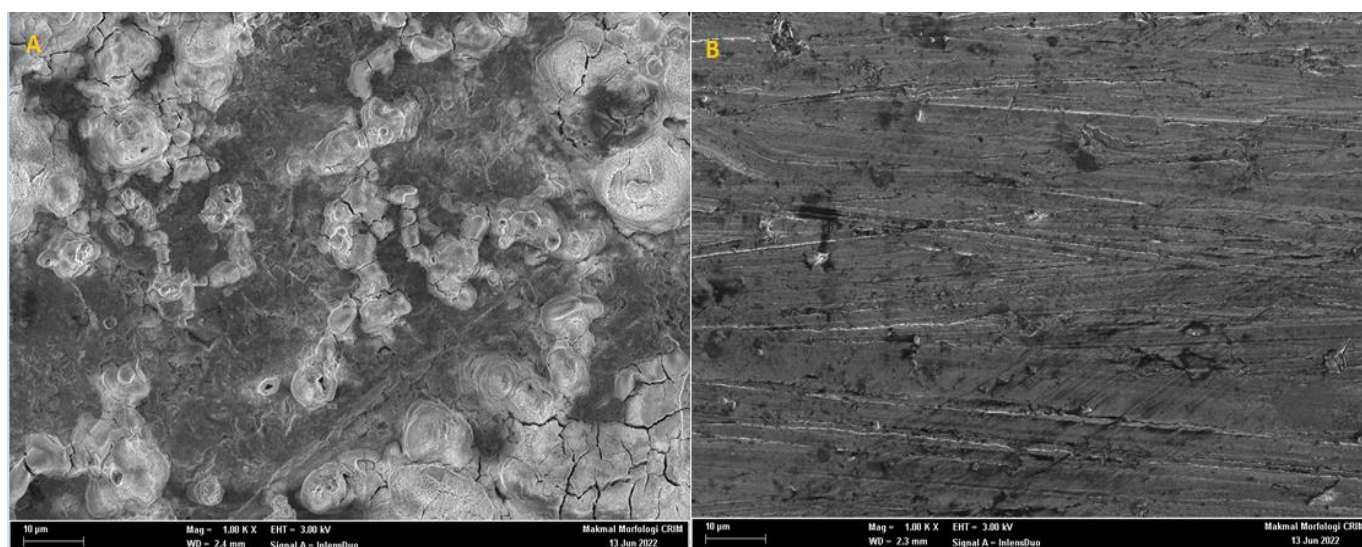


Figure 10. SEM micrographs showing the surface morphology of mild-steel-coupon surface in absence (A) and presence (B) of 0.0005 M PMBMH in 1 M HCl environment for 5 h at 303 K.

2.8. Quantum Chemical Computations

With the use of ChemOffice software, the adsorption ability of the synthesized inhibitor over the mild-steel-coupon surface can be explored from a quantum-chemical-computation standpoint, using frontier molecular orbital theory (FMOT) [47–49]. The donor–acceptor interactions could be at the root of the tested inhibitor’s adsorption. In this situation, electrons are moved from the organic compound’s high-electron-density centers (nitrogen, oxygen, sulfur, and electrons (i.e., regions of highly electronic distributions)) to the mild-steel surface’s unoccupied 3d orbital (iron surface).

Table 5 depicts and discusses the quantum chemical variables acquired from the optimization of the tested inhibitor in the gas phase (shown in Figure 11). The highest occupied-molecular-orbital (E_{HOMO}) energy shows the capability of the tested inhibitor to donate electrons. The capability of the molecules to accept electrons from the back donation of iron, and to thus enhance the binding energy between the metal and the inhibitor, is shown by a lower E_{LUMO} value.

Table 5. Calculated quantum parameters of the studied inhibitor.

E_{HOMO}	E_{LUMO}	ΔE (eV)	A	I	χ (eV)	η (eV)	ΔN (eV)	μ (D)
−8.826	−2.336	6.49	2.336	8.826	5.581	6.49	0.00586	2.7364

The greater the E_{HOMO} and the lower the E_{LUMO} , the better the tested inhibitor’s capacity to attach to the metal surface [50–53]. As seen in Table 5, the E_{HOMO} rises as the number of examined inhibitor compounds rises. This agrees well with the experimental data and implies that PMBMH is an effective corrosion inhibitor [54]. The energy gap (E_{gap}) values determine the chemical response. In terms of the reactivity, the greater the inhibiting efficiency of the molecule, the more reactive it is toward the substrate surface, and the smaller the ΔE gap, the more stable it is. As a result, PMBMH and the Fe substrate create a stable combination. The dipole moment (μ) is caused by the atoms in the molecule having a nonuniform-distribution surface charge. The value of the dipole moment is decreasing, which supports the inhibitor molecule. In the hard–soft acid–base notion, the soft molecule has lower E_{gap} values and higher basicity, and the opposite is true when comparing the hard ones [55]. As a result, the soft molecule has more adsorption ability due to its easier electron transfer, and it is a stronger corrosion inhibitor than the hard molecule.

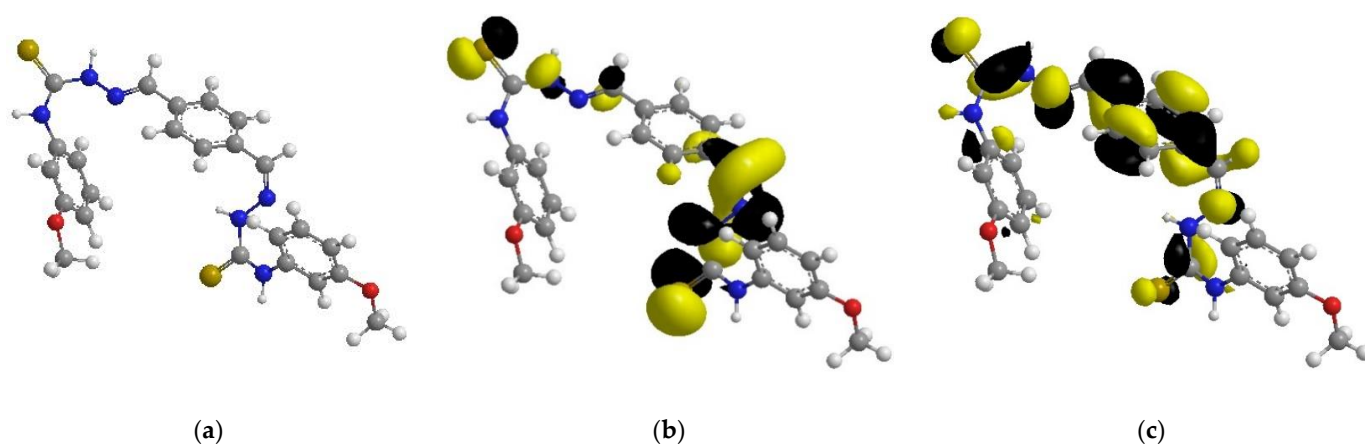


Figure 11. The optimized chemical structure (a), highest occupied molecular orbital (b), and lowest unoccupied molecular orbital (c) of the tested inhibitor.

According to Lukovit's research, when the number of electrons transmitted (ΔN) is less than 3.6, the inhibition performance improves as a function of the electron transfer [56]. The greater the corrosion inhibitor, the larger the fraction of electron transport (ΔN). As shown in Table 5, the ΔN increases as the quantity of ethylene oxide units increases, which confirms the highest adsorption ability of the tested inhibitor, as previously stated by the experimental data. The chemical reactivity of atoms and molecules is represented by the ionization energy. As a result, as the ionization energy rises, the reactivity rises as well, and the inhibition efficiency falls. These data back up the gravimetric readings that were taken.

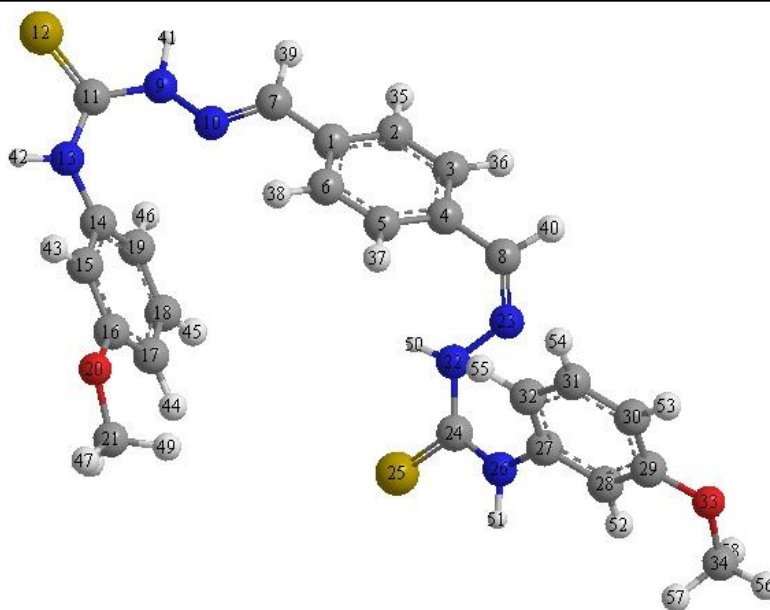
2.9. Mulliken Charges

Mulliken charges were used to determine the adsorption centers of the tested inhibitor [57]. The easier it is for the atoms to transfer electrons, the more negatively charged they are. Table 6 shows that N, O, and S atoms are electron-donating sites in the inhibitor compounds that have been studied. It is obvious from Table 6 that S(25), O(33), N(22), O(20), N(13), S(12), and N(9) have the highest atomic charges (-0.3009 , -0.2084 , -0.2717 , -0.2126 , -0.2595 , -0.2816 , and -0.2638 , respectively). These atoms have the ability to bond with the metal surface and form coordination bonds.

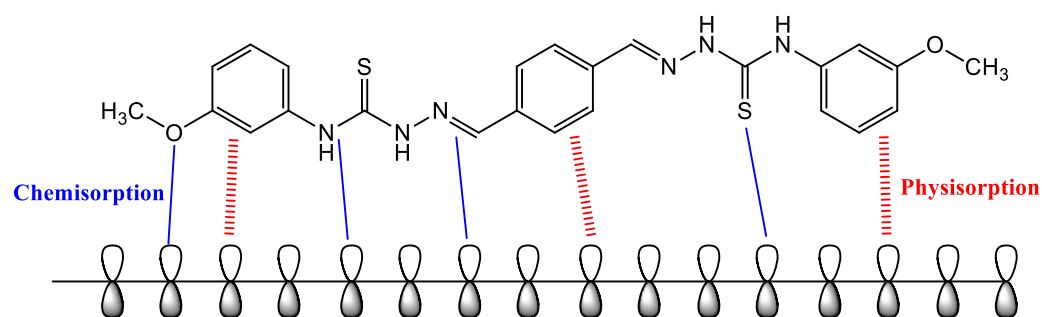
2.10. Suggested Corrosion-Inhibition Mechanism

The creation of a protective layer that is absorbed onto the iron surface is responsible for the inhibitory inertia of organic molecules. The presence of the tested inhibitor significantly reduced the mild-steel corrosion, according to gravimetric tests. Furthermore, the adsorption isotherm analyses show that the adsorption of the studied inhibitor molecules onto the mild-steel surface follows the Langmuir adsorption model quite closely. Furthermore, the generated protective film's adsorption behavior is principally determined by: (1) electrostatic interactions through protonated heteroatoms, and (2) different linkages between inhibitor molecules and the mild-steel surface [58].

The interaction between the tested inhibitor molecules and the mild-steel surface is depicted in further detail in Figure 12. The interaction between both the pi-electrons of the aromatic rings and the empty d-orbital of the metal atoms is the most common technique of adsorption between the inhibitor molecule and the mild-steel surface. The second method is the donor-acceptor interactions between the vacant d-orbital of the iron (mild steel) surface atoms and the lone electron pairs in the heteroatoms (S, O, and N). These active electrons are destined to be shared with the Fe atom's d-orbitals.

Table 6. Mulliken charges of tested inhibitor molecules.

Atoms	Charges								
C(1)	-0.0273	C(8)	-0.1133	C(15)	-0.1824	N(22)	-0.2717	C(29)	0.0979
C(2)	-0.1164	N(9)	-0.2638	C(16)	0.0916	N(23)	-0.0308	C(30)	-0.1626
C(3)	-0.1069	N(10)	-0.0278	C(17)	-0.2022	C(24)	0.1863	C(31)	-0.0843
C(4)	-0.0879	C(11)	0.179	C(18)	-0.081	S(25)	-0.3009	C(32)	-0.1626
C(5)	-0.1256	S(12)	-0.2816	C(19)	-0.1548	N(26)	-0.2613	O(33)	-0.2084
C(6)	-0.0927	N(13)	-0.2595	O(20)	-0.2126	C(27)	0.0914	C(34)	-0.0773
C(7)	-0.1274	C(14)	0.0778	C(21)	-0.0781	C(28)	-0.2309	H(35)	0.1386

**Figure 12.** Suggested corrosion-inhibition mechanism of mild steel in 1 M HCl with the addition of the examined inhibitor.

3. Materials and Methods

3.1. Synthesis of the Corrosion Inhibitor

A solution of terephthalaldehyde (0.1 mmol) in 100 mL ethyl alcohol was refluxed with 4-(meta-methoxyphenyl)-3-thiosemicarbazide (0.2 mmol) for 5 h with a few drops of glacial acetic acid. After cooling to room temperature, a solid mass was separated and recrystallized from ethyl alcohol with an 83% yield. The yellow product (221–223 °C) was characterized by various spectroscopic techniques. IR: 3289.5 and 3139.6 cm^{-1} (N–H, amines), 3079.3 cm^{-1} (C–H, aromatic), 2945.3 cm^{-1} (C–H, aliphatic), 1548.6 cm^{-1} (C=N, imine), 1463.8 cm^{-1} (C=C, aromatic); 1168.7 and 1051.5 cm^{-1} (C–O, sy and asy). $^1\text{H-NMR}$ (DMSO- d_6): δ 3.73 (6H, s, -OCH₃), 6.65 (2H, dd), 7.17–7.46 (6H, d, aromatic ring), 7.57 (4H, dd, aromatic ring), 7.94 (2H, s, -CH=N-), 9.93 (2H, s, NH), and 11.47 (2H, s, NH). $^{13}\text{C NMR}$ (DMSO- d_6): δ 57.2, 107.1, 114.9, 121.3, 129.6, 131.2, 133.7, 134.1, 139.1, 139.9, 159.4, 178.3.

3.2. Mild Steel

The mild-steel-sample elemental analysis used for the gravimeter measurements (wt%) is detailed in Table 7.

Table 7. Mild-steel chemical composition (wt%).

C	Mn	Si	Al	S	P	Fe
0.21%	0.05%	0.38%	0.01%	0.05%	0.09%	balance

3.3. Medium

The solubility of PMBMH was determined in 1 M hydrochloric acid solution. The 1 M corrosive environment was prepared by diluting 37% HCl (Merck-Malaysia) in double-distilled water. The measurements were performed without and with the addition of PMBMH at different concentrations (0.0001, 0.0002, 0.0003, 0.0004, 0.0005, and 0.001 M), with various immersion times (1, 5, 10, 24, and 48 h). The effect of temperature (303, 313, 323, and 333 K) was also studied at various inhibitor concentrations for an immersion time of 5 h.

3.4. Weight-Loss Measurements

The traditional weight-loss measurements were performed according to the procedures described in this article [59–61]. At temperatures ranging from 303 K to 333 K, cleaned, polished, and weighed mild-steel specimens were immersed in a 1 M HCl environment in the absence and presence of varied doses of the tested inhibitor for various exposure times (1, 5, 10, 24, and 48 h). To ensure that the tests could be replicated, each measurement was carried out three times, and only the average results were published. The corrosion rate and inhibition efficiency were calculated from Equations (8) and (9):

$$C_R = \frac{87600W}{atd} \quad (8)$$

where W is the weight loss of the tested mild steel (gram), a is the tested mild-steel surface area (cm^2), t is the exposure time (h), and d is the tested mild-steel density (gcm^{-3});

$$IE\% = \left[\frac{C_{R(o)} - C_{R(i)}}{C_{R(o)}} \times 100 \right] \quad (9)$$

where $C_{R(o)}$ is the rate of corrosion in the absence of PMBMH, and $C_{R(i)}$ is the rate of corrosion in the presence of PMBMH.

3.5. Electrochemical Data

As the working electrodes throughout the study, mild-steel coupons were cleaned in accordance with ASTM standard G1-03 [62]. The coupon's active surface area was 4.5 cm^2 . The experiments were performed in a 1.0 M HCl environment that was aerated but not agitated at 303 K, with tested inhibitor concentrations ranging from 0.0001 to 0.0005 M. To ensure that the tests could be replicated, each measurement was carried out three times, and only the average results were published. A Gamry Instrument Potentiostat/Galvanostat/ZRA type REF 600 was used for the measurements. Gamry's DC105 and EIS300 software was utilized for the electrochemical impedance spectroscopy (EIS) and potentiodynamic scanning, respectively. At a scan rate of 0.5 mVs^{-1} , the potentiodynamic current-potential curves were adjusted from 0.25 to +0.25 V sce. Using the Gamry Echem Analyst program, all of the impedance values were matched to the proper equivalent circuits (ECs). A Gamry water-jacketed glass cell with three electrodes—the working electrode, the counter electrode, and the reference electrode—was used to assess the inhibitory effects of the tested inhibitor. The reference electrode was a saturated calomel electrode

(SCE). Electrochemical tests were started about 30 min after the working electrode was submerged in the solution in order to maintain the steady-state potential [44,63,64].

3.6. Surface Scanning Electron Microscope

Scanning electron microscopy was used to observe the corrosive behavior of the acidic solution (1 M HCl) on the mild-steel surface after 5 h of treatment without and with the addition of 0.0005 M of PMBMH (SEM, Zeiss MERLIN Compact FESEM at the UKM Electron Microscopy Unit).

3.7. Computational Studies

Conceptual computations have recently been performed to simulate experimental findings. ChemOffice was used to perform the quantum chemical computations. We used the conventional theory of Becke's three-parameter hybrid functional (B3LYP) level using a Gaussian 03 version, with 6-31G as the reference set, to investigate the chemical reactivity of the PMBMH molecule. For the synthesized compound (PMBMH in the gas phase), the investigated approach produces the quantum parameters of the energy gap (ΔE), fraction of electron transfer (ΔN), dipole moment (μ), ionization energy (I), electron affinity (A), absolute electronegativity (χ), ionization energy (I), hardness (η), and softness (σ) [65].

The quantum chemical parameters, such as χ , η , σ , and ΔN , were calculated from Equations (10)–(15):

$$I = -E_{HOMO} \quad (10)$$

$$A = -E_{LUMO} \quad (11)$$

$$\chi = \frac{I + A}{2} \quad (12)$$

$$\eta = \frac{I - A}{2} \quad (13)$$

$$\sigma = \frac{1}{\eta} \quad (14)$$

$$\Delta N = \frac{(\chi_{Fe} - \chi_{inh})}{2(\eta_{Fe} - \eta_{inh})} \quad (15)$$

4. Conclusions

Due to the existence of very effective electronic-adsorption centers (S, O, N, and pi-bonds) that block the active centers of iron metal, the examined corrosion inhibitor shows a good corrosion-protection performance for mild steel in 1 M of HCl. The anticorrosion efficiency of PMBMH was studied by weight loss, potentiodynamic polarization, and electrochemical measurements, in addition to quantum chemical calculation. The molecular structure, concentration, and temperature parameters that effect the corrosion inhibition were examined. The following are the key findings:

- PMBMH has the maximum efficiency of 95% at 303 K and is a potential steel corrosion inhibitor in 1.0 M HCl. The heteroatoms and benzene rings in the PMBMH's structure are responsible for its considerable inhibitory efficiency;
- Gravimetric tests showed that the inhibition performance increases with the concentration, with the tested corrosion inhibitor's peak inhibition efficiency being 95% at the ideal concentration (0.0005 M);
- The inhibitor tends to be weakly bonded to the metal surface, and the efficacy of inhibition reduces as the temperature increases. On metallic surfaces, it is anticipated that it will take part in chemical adsorption;
- The electrochemical-experiment findings indicated that PMBMH shields mild-steel corrosion because a shielding inhibitor coating forms at the steel–electrolyte interface;

- The value of the G_{ads} obtained is used to propose chemisorption and physisorption phenomena, and the adsorption process is spontaneous;
- Quantum chemistry simulations demonstrate that the tested inhibitor molecules adsorb onto a mild-steel surface utilizing sulfur, oxygen, and nitrogen heteroatoms, in addition to the pi-electrons of the benzene rings, as their efficient centers;
- As a result, the findings of the experiments and theoretical analysis are in good accord.

Author Contributions: Conceptualization, M.K.A. and M.K.M.; methodology, W.K.A.-a.; software, B.S.M.; validation M.K.A., M.K.M. and B.S.M.; formal analysis, M.M.H.; investigation, M.H.H.A.-k.; resources, M.M.H.; data curation, W.K.A.-a.; writing—original draft preparation, A.A.A.-a. and L.M.S.; writing—review and editing, A.A.A.-a. and L.M.S.; visualization, M.H.H.A.-k.; supervision, W.N.R.W.I., A.A.H.K. and M.S.T.; project administration, funding acquisition, W.N.R.W.I., A.A.H.K. and M.S.T. All authors have read and agreed to the published version of the manuscript.

Funding: This research received no external funding.

Institutional Review Board Statement: Not applicable.

Informed Consent Statement: Not applicable.

Data Availability Statement: Not applicable.

Acknowledgments: The authors acknowledge the Al-Farahidi University and Universiti Kebangsaan Malaysia (UKM) for their support, also we gratefully acknowledges to W.N.R.W.I., for his project (GUP-2020-012).

Conflicts of Interest: The authors declare no conflict of interest.

Sample Availability: Samples of the compounds are available from the authors.

References

1. Yadav, M.; Yadav, P.; Sharma, U. Substituted imidazoles as corrosion inhibitors for N80 steel in hydrochloric acid. *Indian J. Chem. Technol.* **2013**, *20*, 363–370.
2. Zarrok, H.; Assouag, M.; Zarrouk, A.; Oudda, H.; Hallaoui, A.; Touzani, R.; Allali, M.; Hammouti, B.; El Hezzat, M.; Bouachrine, M. Quantum chemical study on the corrosion inhibition of some bipyrazoles. *Res. J. Pharm. Biol. Chem. Sci.* **2015**, *6*, 1853–1860.
3. Gece, G. The use of quantum chemical methods in corrosion inhibitor studies. *Corros. Sci.* **2008**, *50*, 2981–2992. [[CrossRef](#)]
4. Obot, I.B.; Macdonald, D.D.; Gasem, Z.M. Density functional theory (DFT) as a powerful tool for designing new organic corrosion inhibitors. Part 1: An overview. *Corros. Sci.* **2015**, *99*, 1–30. [[CrossRef](#)]
5. Camacho-Mendoza, R.L.; Gutiérrez-Moreno, E.; Guzmán-Percástegui, E.; Aquino-Torres, E.; Cruz-Borbolla, J.; Rodríguez-Ávila, J.A.; Alvarado-Rodríguez, J.G.; Olvera-Neria, O.; Thangarasu, P.; Medina-Franco, J.L. Density Functional Theory and Electrochemical Studies: Structure-Efficiency Relationship on Corrosion Inhibition. *J. Chem. Inf. Model.* **2015**, *55*, 2391–2402. [[CrossRef](#)] [[PubMed](#)]
6. Rubaye, A.; Abdulwahid, A.; Al-Baghdadi, S.B.; Al-Amiery, A.; Kadhum, A.; Mohamad, A. Cheery sticks plant extract as a green corrosion inhibitor complemented with LC-EIS/MS spectroscopy. *Int. J. Electrochem. Sci.* **2015**, *10*, 8200–8209.
7. Bockris, J.O.M.; Reddy, A.K.N. *Modern Electrochemistry*; Plenum Press: New York, NY, USA, 1997; Volume 2.
8. Abdallah, M.; Fawzy, A.; Hawsawi, H.; Hameed, R.S.A.; Al-Juaid, S.S. Estimation of water-soluble polymeric materials (Poloxamer and Pectin) as corrosion inhibitors for carbon steel in acidic medium. *Int. J. Electrochem. Sci.* **2020**, *15*, 8129–8144. [[CrossRef](#)]
9. Abdallah, M.; Hazazi, O.A.; Fawzy, A.; El-Shafei, S.; Fouda, A.S. Influence of N-thiazolyl-2-cyanoacetamide derivatives on the corrosion of aluminum in 0.01M sodium hydroxide. *Prot. Met. Phys. Chem. Surf.* **2014**, *50*, 659–666. [[CrossRef](#)]
10. Issaadi, S.; Douadi, T.; Zouaoui, A.; Chafaa, S.; Khan, M.A.; Bouet, G. Novel thiophene symmetrical Schiff base compounds as corrosion inhibitor for mild steel in acidic media. *Corros. Sci.* **2011**, *53*, 1484–1488. [[CrossRef](#)]
11. Fu, L.; Xiong, Y.; Chen, S.; Long, Y. Trace copper ion detection by the suppressed decolorization of chromotrope 2R complex. *Anal. Methods* **2015**, *7*, 266–270. [[CrossRef](#)]
12. Bockris, J.O.; Swinkels, D.A.J. Adsorption of n-decylamine on solid metal electrodes. *J. Electrochem. Soc.* **1964**, *11*, 736–744. [[CrossRef](#)]
13. Dean, S.W.; Grab, G.D. Corrosion of carbon steel by concentrated sulfuric acid. *Mater. Perform.* **2012**, *58*, 1–11. [[CrossRef](#)]
14. Chaouiki, A.; Chafiq, M.; Lgaz, H.; Al-Hadeethi, M.; Ali, I.; Masroor, S.; Chung, I. Green Corrosion Inhibition of Mild Steel by Hydrazone Derivatives in 1.0 M HCl. *Coatings* **2020**, *10*, 640. [[CrossRef](#)]
15. Jacob, K.; Parameswaran, G. Corrosion inhibition of mild steel in hydrochloric acid solution by Schiff base furoin thiosemicarbazone. *Corros. Sci.* **2010**, *52*, 224–228. [[CrossRef](#)]

16. Xu, B.; Yang, W.; Liu, Y.; Yin, X.; Gong, W.; Chen, Y. Experimental and theoretical evaluation of two pyridinecarboxaldehyde thiosemicarbazone compounds as corrosion inhibitors for mild steel in hydrochloric acid solution. *Corros. Sci.* **2014**, *78*, 260–268. [[CrossRef](#)]
17. Lgaz, H.; Salghi, R.; Jodeh, B.; Hammouti, B. Effect of clozapine on inhibition of mild steel corrosion in 1.0 M HCl medium. *J. Mol. Liq.* **2017**, *225*, 271–280. [[CrossRef](#)]
18. Naciri, M.; El Aoufir, Y.; Lgaz, H.; Lazrak, F.; Ghanimi, A.; Guenbour, A.; Ali, I.; El Moudane, M.; Taoufik, J.; Chung, J. Exploring the potential of a new 1,2,4-triazole derivative for corrosion protection of carbon steel in HCl: A computational and experimental evaluation. *Colloids Surf. A Physicochem. Eng. Asp.* **2020**, *597*, 124604. [[CrossRef](#)]
19. Hsissou, R.; Dagdag, O.; Benhiba, A.; Berradi, M.; El Bouchti, M.; Berisha, A.; Hajjaji, N.; Elharfi, A. Novel derivative epoxy resin TGETET as a corrosion inhibition of E24 carbon steel in 1.0M HCl solution. Experimental and computational (DFT and MD simulations) methods. *J. Mol. Liq.* **2019**, *284*, 182–192. [[CrossRef](#)]
20. Abdelwedoud, B.; Damej, M.; Tassaoui, K.; Berisha, A.; Tachallait, H.; Bougrin, K.; Mehmeti, V.; Benmessaoud, M. Inhibition effect of N-propargyl saccharin as corrosion inhibitor of C38 steel in 1 M HCl, experimental and theoretical study. *J. Mol. Liq.* **2022**, *354*, 118784. [[CrossRef](#)]
21. Azgaou, K.; Damej, M.; El Hajjaji, S.; Sebbar, N.; Elmsellem, H.; Ibrahim, B.; Benmessaoud, M. Synthesis and characterization of N-(2-aminophenyl)-2-(5-methyl-1H-pyrazol-3-yl) acetamide (AMPA) and its use as a corrosion inhibitor for C38 steel in 1 M HCl. Experimental and theoretical study. *J. Mol. Struct.* **2022**, *1266*, 133451. [[CrossRef](#)]
22. Negm, N.; Kandile, N.; Badar, E.; Mohammed, M. Gravimetric and electrochemical evaluation of environmentally friendly nonionic corrosion inhibitors for carbon steel in 1 M HCl. *Corros. Sci.* **2012**, *65*, 94–103. [[CrossRef](#)]
23. Madkour, L.; Kaya, S.; Obot, I. Computational, Monte Carlo simulation and experimental studies of some arylazotriazoles (AATR) and their copper complexes in corrosion inhibition process. *J. Mol. Liq.* **2018**, *260*, 351–374. [[CrossRef](#)]
24. Singh, P.; Srivastava, V.; Quraishi, M. Novel quinoline derivatives as green corrosion inhibitors for mild steel in acidic medium: Electrochemical, SEM, AFM, and XPS studies. *J. Mol. Liq.* **2016**, *216*, 164–173. [[CrossRef](#)]
25. Haque, J.; Ansari, K.R.; Srivastava, V.; Quraishi, M.A.; Obot, I.B. Pyrimidine derivatives as novel acidizing corrosion inhibitors for N80 steel useful for petroleum industry: A combined experimental and theoretical approach. *J. Ind. Eng. Chem.* **2017**, *49*, 176–188. [[CrossRef](#)]
26. Anusuya, N.; Saranya, J.; Sounthari, P.; Zarrouk, A.; Chitr, S. Corrosion inhibition and adsorption behaviour of some bis-pyrimidine derivatives on mild steel in acidic medium. *J. Mol. Liq.* **2017**, *225*, 406–417. [[CrossRef](#)]
27. Li, X.; Deng, S.; Lin, T.; Xie, X.; Du, G. 2-Mercaptopyrimidine as an effective inhibitor for the corrosion of cold rolled steel in HNO₃ solution. *Corros. Sci.* **2017**, *118*, 202–216. [[CrossRef](#)]
28. Al-Baghdadi, S.B.; Al-Amiery, A.A.; Gaaz, T.S.; Kadhum, A.A.H. Terephthalohydrazide and isophthalo-hydrazide as new corrosion inhibitors for mild steel in hydrochloric acid: Experimental and theoretical approaches. *Koroze Ochr. Mater.* **2021**, *65*, 12–22. [[CrossRef](#)]
29. Hanoon, M.M.; Resen, A.M.; Shaker, L.M.; Kadhum, A.A.H.; Al-Amiery, A.A. Corrosion investigation of mild steel in aqueous hydrochloric acid environment using n-(Naphthalen-1yl)-1-(4-pyridinyl)methanimine complemented with antibacterial studies. *Biointerface Res. Appl. Chem.* **2021**, *11*, 9735–9743.
30. Al-Baghdadi, S.; Gaaz, T.S.; Al-Adili, A.; Al-Amiery, A.A.; Takriff, M.S. Experimental studies on corrosion inhibition performance of acetylthiophene thiosemicarbazone for mild steel in HCl complemented with DFT investigation. *Int. J. Low-Carbon Technol.* **2021**, *16*, 181–188. [[CrossRef](#)]
31. Al-Amiery, A.A. Anti-corrosion performance of 2-isonicotinoyl-n-phenylhydrazinecarbothioamide for mild steel hydrochloric acid solution: Insights from experimental measurements and quantum chemical calculations. *Surf. Rev. Lett.* **2021**, *28*, 2050058. [[CrossRef](#)]
32. Obot, I.; Obi-Egbedi, N.; Umoren, S. Adsorption characteristics and corrosion inhibitive properties of clotrimazole for aluminium corrosion in hydrochloric acid. *Int. J. Electrochem. Sci.* **2009**, *4*, 863–877.
33. Sliem, M.H.; El Basiony, N.M.; Zaki, E.G.; Sharaf, M.A.; Abdullah, A.M. Corrosion Inhibition of Mild Steel in Sulfuric Acid by a Newly Synthesized Schiff Base: An Electrochemical, DFT, and Monte Carlo Simulation Study. *Electroanalysis* **2020**, *32*, 3145–3158. [[CrossRef](#)]
34. Obot, I.; Obi-Egbedi, N.; Umoren, S. Antifungal drugs as corrosion inhibitors for aluminium in 0.1 M HCl. *Corros. Sci.* **2009**, *51*, 1868–1875. [[CrossRef](#)]
35. Quraishi, M.; Ansari, F.; Jamal, D. Thiourea derivatives as corrosion inhibitors for mild steel in formic acid. *Mater. Chem. Phys.* **2003**, *77*, 687–690. [[CrossRef](#)]
36. Popova, A. Temperature effect on mild steel corrosion in acid media in presence of azoles. *Corros. Sci.* **2007**, *49*, 2144–2158. [[CrossRef](#)]
37. Li, W.; He, Q.; Zhang, S.; Pei, C.; Hou, B. Some new triazole derivatives as inhibitors for mildsteel corrosion in acidic medium. *J. Appl. Electrochem.* **2008**, *38*, 289–295. [[CrossRef](#)]
38. Ferreira, E.S.; Giacomelli, C.; Giacomelli, F.C.; Spinelli, A. Evaluation of the inhibitor effect of L-ascorbic acid on the corrosion of mild steel. *Mater. Chem. Phys.* **2004**, *83*, 129–134. [[CrossRef](#)]
39. Ramesh Saliyan, V.; Adhikari, A.V. Quinolin-5-ylmethylene-3-[[8-(trifluoromethyl)quinolin-4-yl]thio]propanohydrazide as an effective inhibitor of mild steel corrosion in HCl solution. *Corros. Sci.* **2008**, *50*, 55–61. [[CrossRef](#)]

40. Pardo, A.; Merino, M.C.; Arrabal, R.; Feliu, S., Jr.; Viejo, F.; Carboneras, M. Enhanced corrosion resistance of A3xx.x/SiCp composites in chloride media by La surface treatments. *Electrochim. Acta.* **2006**, *51*, 4367–4378. [[CrossRef](#)]
41. Popova, A.; Christov, M. Evaluation of impedance measurements on mild steel corrosion in acid media in the presence of heterocyclic compounds. *Corros. Sci.* **2005**, *48*, 3208–3221. [[CrossRef](#)]
42. Khaled, K.F. The inhibition of benzimidazole derivatives on corrosion of iron in 1 M HCl solutions. *Electrochim. Acta* **2003**, *48*, 2493–2503. [[CrossRef](#)]
43. Hleli, S.; Abdelghani, A.; Tlili, A. Impedance spectroscopy technique for DNA hybridization. *Sensors* **2003**, *3*, 472–479. [[CrossRef](#)]
44. Meyer, Y.A.; Menezes, I.; Bonatti, R.S.; Bortolozzo, A.D.; Osório, W.R. EIS Investigation of the Corrosion Behavior of Steel Bars Embedded into Modified Concretes with Eggshell Contents. *Metals* **2022**, *12*, 417. [[CrossRef](#)]
45. Bonatti, R.S.; Meyer, Y.A.; Padilha, P.G.; Bortolozzo, P.A.; Osório, W.R. Silicon Content Affecting Corrosion Behavior of Alp/Sip Composites in a Biodiesel Blend. *Corrosion* **2020**, *76*, 1109–1121. [[CrossRef](#)]
46. Duarte, T.; Meyer, Y.A.; Osório, W.R. The Holes of Zn Phosphate and Hot Dip Galvanizing on Electrochemical Behaviors of Multi-Coatings on Steel Substrates. *Metals* **2022**, *12*, 863. [[CrossRef](#)]
47. Fu, J.; Zang, H.; Wang, Y.; Li, S.; Chen, T.; Liu, X. Experimental and theoretical study on the inhibition performances of quinoxaline and its derivatives for the corrosion of mild steel in hydrochloric acid. *Ind. Eng. Chem. Res.* **2012**, *51*, 6377–6386. [[CrossRef](#)]
48. Saha, S.K.; Ghosh, P.; Hens, A.; Murmu, N.C.; Banerjee, P. Density functional theory and molecular dynamics simulation study on corrosion inhibition performance of mild steel by mercapto-quinoline Schiff base corrosion inhibitor. *Physica E* **2015**, *66*, 332–341. [[CrossRef](#)]
49. Fouda, A.S.; Ismail, M.A.; Temraz, A.M.; Abousalem, A.S. Comprehensive investigations on the action of cationic terthiophene and bithiophene as corrosion inhibitors: Experimental and theoretical studies. *New J. Chem.* **2019**, *43*, 768–789. [[CrossRef](#)]
50. Saha, S.K.; Banerjee, P. Introduction of newly synthesized Schiff base molecules as efficient corrosion inhibitors for mild steel in 1 M HCl medium: An experimental, density functional theory and molecular dynamics simulation study. *Mater. Chem. Front.* **2018**, *2*, 1674–1691. [[CrossRef](#)]
51. Chen, R.; Fan, F.; Dittrich, T.; Li, C. Imaging photogenerated charge carriers on surfaces and interfaces of photocatalysts with surface photovoltage microscopy. *Chem. Soc. Rev.* **2018**, *47*, 8238–8262. [[CrossRef](#)]
52. Guo, L.; Obot, I.B.; Zheng, X.; Shen, X.; Qiang, Y.; Kaya, S.; Kaya, C. Theoretical insight into an empirical rule about organic corrosion inhibitors containing nitrogen, oxygen, and sulfur atoms. *Appl. Surf. Sci.* **2017**, *406*, 301–306. [[CrossRef](#)]
53. Masoud, M.; Awad, M.; Shaker, M.; El-Tahawy, M. The role of structural chemistry in the inhibitive performance of some aminopyrimidines on the corrosion of steel. *Corros. Sci.* **2010**, *52*, 2387–2396. [[CrossRef](#)]
54. Mert, B.D.; Yüce, A.O.; Kardaş, G.; Yazıcı, B. Inhibition effect of 2-amino-4-methylpyridine on mild steel corrosion: Experimental and theoretical investigation. *Corros. Sci.* **2014**, *85*, 287–295. [[CrossRef](#)]
55. Labjar, N.; Bentiss, F.; Lebrini, M.; Jama, C.; El hajjaji, S. Study of Temperature Effect on the Corrosion Inhibition of C38 Carbon Steel Using Amino-tris(Methylenephosphonic) Acid in Hydrochloric Acid Solution. *Int. J. Corros.* **2011**, *2011*, 548528. [[CrossRef](#)]
56. Al-Sabagh, A.; El Basiony, N.; Sadeek, S.; Migahed, M. Scale and corrosion inhibition performance of the newly synthesized anionic surfactant in desalination plants: Experimental, and theoretical investigations. *Desalination* **2018**, *437*, 45–58. [[CrossRef](#)]
57. Ebenso, E.E.; Arslan, T.; Kandemirli, F.; Caner, N.; Love, I. Quantum chemical studies of some rhodanine azosulpha drugs as corrosion inhibitors for mild steel in acidic medium. *Int. J. Quantum Chem.* **2010**, *110*, 1003–1018. [[CrossRef](#)]
58. Assad, N.; Abdul-Hameed, F.; Yousif, E.; Balakit, A. Synthesis of Thiophene Derivative and its Use as Zinc Metal Corrosion Inhibitor in Hydrochloric Acid Solution. *ANJS* **2018**, *18*, 69–78. [[CrossRef](#)]
59. Alamiery, A.A.; Wan Isahak, W.N.R.; Takriff, M.S. Inhibition of Mild Steel Corrosion by 4-benzyl-1-(4-oxo-4-phenylbutanoyl)thiosemicarbazide: Gravimetric, Adsorption and Theoretical Studies. *Lubricants* **2021**, *9*, 93. [[CrossRef](#)]
60. Ramya, K.; Mohan, R.; Anupama, K.K. Abraham Joseph, Electrochemical and theoretical studies on the synergistic interaction and corrosion inhibition of alkyl benzimidazoles and thiosemicarbazide pair on mild steel in hydrochloric acid. *Mater. Chem. Phys.* **2015**, *149–150*, 632–647. [[CrossRef](#)]
61. TM0193-2016-SG; NACE International, Laboratory Corrosion Testing of Metals in Static Chemical Cleaning Solutions at Temperatures below 93 °C (200 °F), The standard procedure for immersion testing as detailed in NACE TM0169/G31. 2000.
62. ASTM G-31-72; Standard Recommended Practice for the Laboratory Immersion Corrosion Testing of Metals. ASTM: Philadelphia, PA, USA, 1990; p. 401.
63. Zhang, X.L.; Jiang, Z.H.; Yao, Z.P.; Song, Y.; Wu, Z.D. Effects of scan rate on the potentiodynamic polarization curve obtained to determine the Tafel slopes and corrosion current density. *Corros. Sci.* **2009**, *51*, 581–587. [[CrossRef](#)]
64. McCafferty, E. Validation of corrosion rates measured by Tafel extrapolation method. *Corros. Sci.* **2005**, *47*, 3202–3215. [[CrossRef](#)]
65. Koopmans, T. Ordering of wave functions and eigenenergy's to the individual electrons of an atom. *Physica* **1933**, *1*, 104–113. [[CrossRef](#)]